Computation

CrossMark

Effect of micro-cracks on plastic zone ahead of the macro-crack tip

Li Xiaotao[1,*], Li Xu[1], Yang Hongda[1], and Jiang Xiaoyu[1]

[1] School of Mechanics and Engineering, Southwest Jiaotong University, Chengdu 610031, China

ABSTRACT

From the macroscopic point of view, the plastic zone (PZ) is obtained based on the distributed dislocation technique (DDT) and von Mises yield criterion. From the microscopic point of view, PZ is determined by the DDT model. The effect of micro-cracks on PZ of the macro-crack tip is analyzed. The results show that the micro-crack has a little amplification effect on PZ of the macro-crack tip when it locates in front of PZ. As the micro-crack is close to the macro-crack tip, PZ of the macro-crack tip and the micro-crack tip will join together. When the micro-crack enters into PZ of the macro-crack tip, it has an obvious shielding effect on PZ. When the micro-crack is behind the macro-crack tip, the width of PZ decreases while the height increases. The dislocation distribution in PZ is in the form of inverse pileup. The amplification and shielding regions are divided into five strip-shaped regions, and they appear alternately. The results can provide useful information to predict plastic behaviors near crack tip. The analysis of amplification and shielding effect is important to materials design.

Introduction

The fatigue and fracture of materials have been widely investigated since last century. The linear elastic fracture mechanics (LEFM) have been a mature tool to solve many crack problems. According to LEFM, the behaviors of materials are linear elastic, so the stresses at the crack tip are singular. In fact, the material will yield and generate a PZ when the stress near the crack tip exceeds the yield limit of the material. When it is small-scale yielding, LEFM can be still applied to analyze behaviors of the materials containing cracks. For the brittle fracture and fatigue crack problem, a little plastic deformation will occur.

The stress intensity factor is an important mechanical parameter to study these problems. However, PZ will increase as the external load increases. LEFM cannot be applied to solve crack problems when PZ size is relatively large and it is large-scale yielding. In this case, the mechanical parameters J integral [1] and crack tip open displacement were proposed to be the fracture criterions. There is a positive correlation among J integral, crack tip open displacement and PZ size [1–4]. So it is necessary to investigate PZ at the crack tip.

From the macroscopic point of view, PZ is predicted by the yield criterions, such as von Mises, Tresca, Hill yield criterion and so on. Considering

Address correspondence to E-mail: 1293657604@qq.com

T-stress or complete stress field, Sousa et al. [5] calculated PZ of the crack tip based on von Mises yield criterion. Vasco-Olmo et al. [6] studied the shape and size using both von Mises yield criterion and Tresca yield criterion and analyzed the influence of PZ on the crack tip shielding. Xin et al. [7] investigated PZ of the crack tip based on Hill yield criterion for orthotropic materials and isotropic materials. Nazarali and Wang [8] analyzed the effect of T-stress on PZ of the crack tip based on von Mises yield criterion. Based on the finite element method, Caputo et al. [9] investigated the effect of the loading conditions, the yield limit, the crack length and the thickness on PZ size. Chen et al. [10] analyzed the relationship between cyclic PZ size and the maximum crack opening displacement. Bouiadjra et al. [11, 12] studied the effect of microcracks and microcavities on PZ shape and size of the macro-crack tip. Paul [13] analyzed the influence of the inclusion on PZ of the crack tip. Based on experimental method, Korda et al. [14] observed cyclic PZ by in situ scanning electron microscope for high-strength steels. Mishra and Parida [15] studied PZ at a center crack tip in a thin sheet by the photostress coating method.

From the microscopic point of view, actually, the plastic deformation at the crack tip is due to dislocations emitted from the crack tip. Ding et al. [16], Saka and Agata [17], Goswami and Pande [18] and Ohr el al. [19–22] observed the dislocations at the crack tip by experiments. Some theoretical dislocation models were proposed to explain the micromechanism of PZ. Bilby et al. [23] proposed the famous BCS model that the yield zone was represented by continuously distributed dislocations along the crack line. Chang and Ohr [24] improved BCS model and proposed the dislocation-free zone model. The model considered that there was an elastic zone between the crack tip and PZ, which was observed by transmission electron microscope fracture experiments [18, 19, 22]. Lung and Xiong [25] proposed a negative dislocation model to modify BCS model. Atkinson and Kanninen [26, 27] proposed an inclined strip yield super-dislocation model. Chen and Takezono [28] and Lee and Chung [29] presented the inclined strip yield continuous dislocation model. The results [23–26] shown that these dislocation models have certain limitations to represent the shape of PZ, but they are valid to calculate PZ size and the crack tip open displacement.

It is difficult to avoid generating micro-cracks in the process of material manufacture and application. So the interaction problem between the micro-cracks and the macro-crack was widely investigated. Kachanov [30–32] proposed a simple solution to crack problems that the actual tractions on individual cracks were replaced approximately by the average tractions. Gong et al. [33–35], Horiand and Nemat-Nasser [36] and Meguid et al. [37] studied the interaction between micro-cracks and the macro-crack based on the complex potentials method. Ibbett et al. [38] investigated the effect of the particles on the crack propagation by the extended finite element method. In order to analyze complex crack problems effectively, DDT was proposed and it was introduced in detail by the book [39]. Its core idea was that the cracks and boundaries could be replaced by the continuously distributed dislocations. Based on DDT, Han and Dhanasekar [40], Zhang et al. [41] and Li et al. [42] presented the solution of a finite plane containing cracks. Jin and Keer [43] studied interaction among multiple edge cracks. Li et al. [44] considered the effect of the micro-crack on the macro-crack propagation in an infinite plane. The influence of the defects on PZ ahead of the crack tip was investigated by some researchers based on DDT, and Chang and Kotousov [45] presented a strip yield model for two collinear cracks. Hoh et al. [46] investigated the effect of a circular inclusion on the crack tip plasticity.

The fore-mentioned works investigated the interaction between the macro-crack and micro-cracks by theoretical method, but they did not consider the plasticity of the crack tip. When the plasticity was considered, they utilized only the finite element method to analyze interaction problem between the macro-crack and micro-cracks. In this way, the micromechanism of interaction between the micro-cracks and PZ ahead of the macro-crack tip cannot be understood clearly. In the paper, the influence of the micro-cracks on PZ of the macro-crack tip is investigated based on DDT and the Gauss–Chebyshev quadrature method. PZ is determined based on von Mises yield criterion, and the effect of the micro-crack on PZ shape and size is analyzed. On the other hand, the DDT model is established to model PZ. The dislocation density is obtained, and the influence of the micro-crack on PZ size of the macro-crack tip is analyzed.

Formulation

In the paper, PZ of the macro-crack tip in the presence of the micro-crack is determined by von Mises yield criterion and the DDT model.

PZ based on von Mises yield criterion

Problem description

As shown in Fig. 1, an infinite plane contains an arbitrarily oriented micro-crack and a macro-crack under uniaxial tension load.

The infinite plane is assumed to be elastic. The cracks can be replaced by the continuously distributed dislocations based on DDT. The problem can be equivalent to two subproblems. The first one is that an infinite plane without the cracks is subjected to remote uniaxial tension load. The second is that an infinite plane contains continuously distributed dislocations in the crack regions without external load. So the stresses at an arbitrary location can be obtained. Based on von Mises yield criterion, the yield zone can be determined. θ and α are shown in Fig. 1, and the positive values are defined in the anticlockwise direction. θ and α are called as the micro-crack orientation and the micro-crack angle, respectively.

Solution scheme

As described in "Problem description" section, the problem shown in Fig. 1 can be equivalent to two
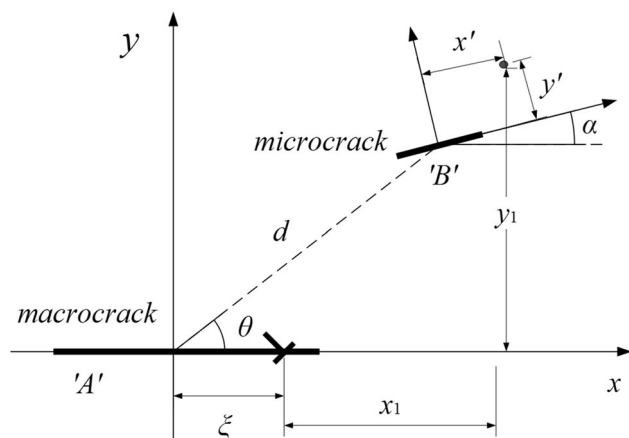
Figure 1 An infinite plane containing a micro-crack and a macro-crack under uniaxial tension load.

subproblems. Firstly, the solution to the second subproblem will be presented. An edge dislocation with the components of Burgers vector b_x and b_y is located at the position $(\xi, 0)$ in an infinite plane. The stress components at the position (x, y) due to the dislocation can be given by

$$\bar{\sigma}_{ij}(\xi, x, y) = c\left[b_x G_{xij}(\xi, x, y) + b_y G_{yij}(\xi, x, y)\right] \\ ij = xx,\ xy\ or\ yy \tag{1}$$

where $c = 2\mu/\pi(\kappa + 1)$. μ is shear modulus. κ is Kolosov's constant and $\kappa = (3 - v)/(1 + v)$ in plane stress, v being Poisson's ratio. $\boldsymbol{G}(\xi, x, y)$ is the dislocation influence function. The first subscript on $\boldsymbol{G}(\xi, x, y)$ denotes the Burgers vector, and the last two denote the associated tractions. The expressions of $\boldsymbol{G}(\xi, x, y)$ can be obtained by the book [39].

In order to convenient statement, the macro-crack is called as crack A and the micro-crack is called as crack B. The stresses in the global coordinate system x–o–y at the point $(x_1 + \xi, y_1)$ induced by the dislocation can be given by

$$\bar{\sigma}_{ij}(x', y', \xi) = c\left\{b_x G^{AB}_{xij}(x_1, y_1) + b_y G^{AB}_{yij}(x_1, y_1)\right\} \\ ij = xx,\ xy\ or\ yy \tag{2}$$

where

$$x_1 = d\cos\theta - \xi + x'\cos\alpha - y'\sin\alpha; \\ y_1 = d\sin\theta + x'\sin\alpha + y'\cos\alpha \tag{3}$$

The tractions in the local coordinate system x'–o'–y' can be obtained by

$$\bar{\sigma}_{ij}(x', y', \xi) = c\left\{b_x G^{AB}_{xij}(x', y', \xi) + b_y G^{AB}_{yij}(x', y', \xi)\right\} \\ ij = x'y'\ or\ y'y' \tag{4}$$

where

$$G^{AB}_{iy'y'}(x', y', \xi) = G^{AB}_{ixx}(x_1, y_1)\sin^2\alpha + G^{AB}_{iyy}(x_1, y_1)\cos^2\alpha \\ - G^{AB}_{ixy}(x_1, y_1)\sin 2\alpha \\ G^{AB}_{ix'y'}(x', y', \xi) = \left[G^{AB}_{iyy}(x_1, y_1) - G^{AB}_{ixx}(x_1, y_1)\right]\sin\alpha\cos\alpha \\ + G^{AB}_{ixy}(x_1, y_1)\cos 2\alpha \quad i = x\ or\ y \tag{5}$$

For formula (4), setting $y' = 0$, the associated tractions on crack B due to the dislocation along crack A can be obtained. Setting $y' = 0$, $d = 0$ and $\theta = \alpha = 0$, the associated tractions on crack A due to the dislocation along crack A can be obtained. In the same way, the associated tractions on crack A due to the dislocation along crack B can be obtained, and the

associated tractions on crack B due to the dislocation along crack B can be obtained.

Numerical solution of integral equations

Based on the DDT, the micro-crack and the macro-crack can be modeled by continuously distributed dislocations. So the tractions along crack B induced by the total dislocations along crack A and crack B can be given by

$$
\begin{aligned}
\bar{\sigma}_{ij}^{B}(x') =\, &c \int_{-a_A}^{a_A} \left[B_x^A(\xi) G_{xij}^{AB}(x',\xi) + B_y^A(\xi) G_{yij}^{AB}(x',\xi) \right] d\xi \\
&+ c \int_{-a_B}^{a_B} \left[B_x^B(\xi) G_{xij}^{BB}(x',\xi) + B_y^B(\xi) G_{yij}^{BB}(x',\xi) \right] d\xi \\
&ij = x'y' \, or \, y'y'
\end{aligned}
\tag{6}
$$

where $B^A(\xi)$ and $B^B(\xi)$ are the dislocation density of crack A and crack B, respectively. a_A and a_B are the half length of crack A and crack B, respectively. In the same way, the tractions components on crack A due to the total dislocations along crack B and crack A can be obtained.

The first subproblem shown is that an infinite plane without cracks is subjected to remote uniaxial tension load σ^∞. It must ensure that the crack face is traction-free, so the integral equations can be established based on the superposition principle.

$$
\begin{aligned}
\sigma_{ij}^A(x) + \bar{\sigma}_{ij}^A(x) = 0 \quad -a_A < x < a_A; \quad ij = yy \, or \, xy \\
\sigma_{ij}^B(x') + \bar{\sigma}_{ij}^B(x') = 0 \quad -a_B < x' < a_B; \quad ij = y'y' \, or \, x'y'
\end{aligned}
\tag{7}
$$

where

$$
\begin{aligned}
\sigma_{yy}^A(x) = \sigma^\infty; \quad \sigma_{xy}^A(x) = 0; \quad \sigma_{y'y'}^B(x') = \sigma^\infty \cos^2 \alpha; \\
\sigma_{x'y'}^B(x') = \sigma^\infty \sin \alpha \cos \alpha
\end{aligned}
\tag{8}
$$

The analytical solution of singular integral Eq. (7) is difficult to obtain, but the numerical solution can be obtained by Gauss–Chebyshev quadrature method [47, 48]. The cracks are 'singular at both ends,' so the form of dislocation density function may be given by

$$
B(s) = \phi(s) \Big/ \sqrt{(1 - s^2)}
\tag{9}
$$

where $\phi(s)$ is an unknown function. And then Eq. (7) can be replaced approximately by a series of algebraic equations. It can be written as

$$
\begin{aligned}
-\frac{\pi}{c}\sigma_{ij}^\infty(x) = \frac{1}{N}\sum_{I=1}^{N} &\Big\{ a_A \left[\phi_x^A(s_I) G_{xij}^{AA}(t_k, s_I) + \phi_y^A(s_I) G_{yij}^{AA}(t_k, s_I) \right] \\
&+ a_B \left[\phi_{x'}^B(s_I) G_{x'ij}^{BA}(t_k, s_I) + \phi_{y'}^B(s_I) G_{y'ij}^{BA}(t_k, s_I) \right] \Big\} \quad ij = yy \, or \, xy \\
-\frac{\pi}{c}\sigma_{ij}^\infty(x') = \frac{1}{N}\sum_{I=1}^{N} &\Big\{ a_A \left[\phi_x^A(s_I) G_{xij}^{AB}(t_k, s_I) + \phi_y^A(s_I) G_{yij}^{AB}(t_k, s_I) \right] \\
&+ a_B \left[\phi_{x'}^B(s_I) G_{x'ij}^{BB}(t_k, s_I) + \phi_{y'}^B(s_I) G_{y'ij}^{BB}(t_k, s_I) \right] \Big\} \quad ij = y'y' \, or \, x'y'
\end{aligned}
\tag{10}
$$

where

$$
\begin{aligned}
s_I = \cos[\pi(2I-1)/2N] \quad I = 1, 2, \dots, N \\
t_k = \cos[\pi k/N] \quad k = 1, 2, \dots, N-1
\end{aligned}
\tag{11}
$$

The extra equations must be established to solve Eq. (10). Notice that, on the crack, there is no net dislocation.

$$
\sum_{I=1}^{N} \phi_x^A(s_I) = \sum_{I=1}^{N} \phi_y^A(s_I) = \sum_{I=1}^{N} \phi_{x'}^B(s_I) = \sum_{I=1}^{N} \phi_{y'}^B(s_I) = 0
\tag{12}
$$

So Eq. (10) can be solved and $\phi(s_I)$ can be obtained. Further, the stress components at an arbitrary point (x, y) can be given by

$$
\begin{aligned}
\sigma_{ij}(x,y) = \frac{1}{N} c \sum_{I=1}^{N} &\Big\{ a_A \left[\phi_x^A(s_I) G_{xij}(x,y) + \phi_y^A(s_I) G_{yij}(x,y) \right] \\
&+ a_B \left[\phi_{x'}^B(s_I) G_{x'ij}(x,y) + \phi_{y'}^B(s_I) G_{y'ij}(x,y) \right] \Big\} \\
&+ \sigma_{ij}^\infty \quad ij = xx, \, xy \, or \, yy
\end{aligned}
\tag{13}
$$

where $\sigma_{yy}^\infty = \sigma^\infty$ and $\sigma_{xx}^\infty = \sigma_{xy}^\infty = 0$. PZ can be obtained by yield criterion. Considering the case of plane stress, the von Mises yield criterion is given by

$$
(\sigma_1 - \sigma_2)^2 + (\sigma_2)^2 + (\sigma_1)^2 = 2\sigma_f^2
\tag{14}
$$

where σ_f is the yield limit and

$$
\begin{aligned}
\sigma_{1,2} = \frac{1}{2} &\left(\sigma_{xx}(x,y) + \sigma_{yy}(x,y) \right) \\
&\pm \frac{1}{2} \sqrt{\left(\sigma_{xx}(x,y) - \sigma_{yy}(x,y) \right)^2 + 4\sigma_{xy}^2(x,y)}
\end{aligned}
\tag{15}
$$

Substituting Eqs. (13) and (15) into (14), the boundary of PZ can be obtained.

PZ based on the DDT model

Problem description

In the section, PZ is modeled by the distributed dislocation technique, which is called as the DDT model.

As shown in Fig. 2, an infinite plane contains a finite macro-crack, a pair of symmetric micro-cracks and two plastic strips under uniaxial tension load σ^∞. The edge dislocations are emitted from the macro-crack tip. And PZ will be generated at the macro-crack tip under remote uniform tension load. In order to solve the problem, some assumptions and simplifications are made as follows:

1. The material is assumed to be elastic–perfectly plastic, namely that the tensile stress σ_{yy} in PZ is equal to the yield limit.
2. The plasticity at the micro-cracks tip is neglected, because PZ at the micro-cracks tip is relatively small.
3. The edge dislocations in PZs are distributed continuously along the line of the macro-crack.

The cracks can be replaced by the continuously distributed dislocations based on DDT. In order to narrate conveniently, PZs, the macro-crack and the micro-cracks are marked as '1,' '2,' '3,' '4' and '5,' respectively, as shown in Fig. 2. The problem can be equivalent to two subproblems. The first one is that an infinite plane without the macro-crack and the micro-cracks is subjected to remote uniform tension load. The second is that an infinite plane contains continuously distributed dislocations in five regions without external load.

Solution scheme

Firstly, the solution to the second subproblem will be presented. The stresses at point $(x_i, 0)$ in region 'i' induced by the dislocation at location $(\xi_j, 0)$ along region 'j' can be given by
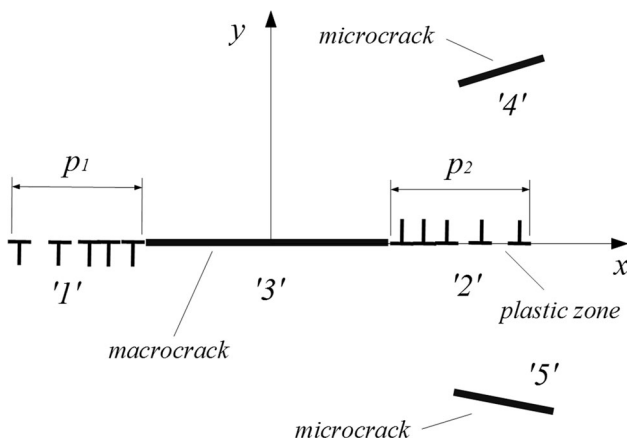
Figure 2 An infinite plane containing a finite macro-crack and a pair of symmetric micro-cracks under uniaxial tension load.

$$\bar{\sigma}_{nm}^{ji}(x_i) = c\left\{b_{x_j}G_{x_jmn}^{ji}(\xi_j, x_i) + b_{y_j}G_{y_jmn}^{ji}(\xi_j, x_i)\right\}$$
$$mn = xy\ or\ yy \tag{16}$$

Based on the principle of superposition, the stresses along region 'i' induced by the all dislocations in five regions can be given by

$$\bar{\sigma}_{mn}^{i}(x_i) = c\sum_{j=1}^{5}\int_{-R_j}^{R_j}\left\{B_{x_j}(\xi_j)G_{x_jmn}^{ji}(\xi_j, x_i) + B_{y_j}(\xi_j)G_{y_jmn}^{ji}(\xi_j, x_i)\right\}d\xi_j$$
$$mn = xy\ or\ yy$$
$$\tag{17}$$

where R_j is the half length of the region 'j.' $R_1 = 0.5p_1$, $R_2 = 0.5p_2$, $R_3 = a_1$ and $R_4 = R_5 = a_2$. $B(\xi_j)$ is the dislocation density function of the region 'j.' For two arbitrarily oriented and located cracks, the dislocation influence functions $G(d, \theta, \alpha)$ have been given by "PZ based on von Mises yield criterion" section. So the dislocation influence function $G^{ji}(\xi_j, x_j)$ in this problem can be obtained by substituting the parameters d, θ and α into d_{ji}, θ_{ji} and α_{ji}. $G^{ji}(\xi_j, x_j) = G^{ji}(\xi_j, x_j, R_j, d_{ji}, \theta_{ji}, \alpha_{ji})$, and the parameters d_{ji}, θ_{ji} and α_{ji} are given in Table 1.

Where p_1 is PZ size of the left tip of the macro-crack and p_2 is PZ size of the right tip. a_1 and a_2 are the half length of the macro-crack and the micro-cracks, respectively. The definition of the parameters d, θ and α is same to Fig. 1. d is the distance between the macro-crack center and the micro-crack center.

Numerical solution of integral equations

For the problem shown in Fig. 2, the cracks face must be ensured traction-free. And the tensile stress σ_{yy} in

Table 1 Parameters d_{ji}, θ_{ji} and α_{ji} in this model

Ji	α_{ji}	d_{ji}	θ_{ji}
11	0	0	0
12	0	$0.5p_1 + 0.5p_2 + 2a_1$	0
13	0	$0.5p_1 + a_1$	0
14	α	$[(d_{13})^2 + d^2 + 2d\,d_{13}\cos\theta]^{0.5}$	$\sin^{-1}[d\sin\theta/d_{41}]$
15	$-\alpha$	$[(d_{13})^2 + d^2 + 2d\,d_{13}\cos\theta]^{0.5}$	$-\sin^{-1}[d\sin\theta/d_{41}]$
22	0	0	0
23	0	$0.5p_2 + a_1$	π
24	α	$[(d_{23})^2 + d^2 - 2d\,d_{23}\cos\theta]^{0.5}$	$\pi - \sin^{-1}[d\sin\theta/d_{42}]$
25	$-\alpha$	$[(d_{23})^2 + d^2 - 2d\,d_{23}\cos\theta]^{0.5}$	$\sin^{-1}[d\sin\theta/d_{42}] - \pi$
33	0	0	0
34	α	d	θ
35	$-\alpha$	d	$-\theta$
44	0	0	0
45	-2α	$d\sin\theta$	$\alpha + 0.5\pi$
55	0	0	0

PZs is equal to the yield limit. So the integral equations can be established as follows.

$$-\frac{\pi}{c}\sigma_{mn}^i(x) = \frac{1}{\pi}\sum_{j=1}^{5}\int_{-R_j}^{R_j}\left\{B_{x_j}(\xi_j)G_{x_jmn}^{ji}(\xi_j,x_i) + B_{y_j}(\xi_j)G_{y_jmn}^{ji}(\xi_j,x_i)\right\}d\xi_j$$

$$mn = xy \, or \, yy$$

(18)

where

$$\sigma_{yy}^1(x) = \sigma_{yy}^2(x) = \sigma^\infty - \sigma_f; \; \sigma_{yy}^3(x) = \sigma^\infty;$$
$$\sigma_{yy}^4(x) = \sigma_{yy}^5(x) = \sigma^\infty\cos^2(\alpha)$$
$$\sigma_{xy}^1(x) = \sigma_{xy}^2(x) = \sigma_{xy}^3(x) = 0;$$
$$\sigma_{xy}^4(x) = \sigma_{xy}^5(x) = \sigma^\infty\cos\alpha\sin\alpha$$

(19)

where σ^∞ and σ_f are the remote tension load and the yield limit, respectively. The analytical solution of Eq. (18) is difficult to be obtained, but its numerical solution can be obtained by Gauss–Chebyshev quadrature method [47, 48]. For the macro-crack and the micro-crack, they are singular at their both ends. So the form of the dislocation density functions can be given by

$$B_j(s) = \phi(s_j)\Big/\sqrt{(1-s_j^2)} \quad j = 3,4,5$$

(20)

For the PZs, they are bounded at their both ends. So the form of the dislocation density functions can be given by

$$B_j(s) = \phi(s_j)\sqrt{(1-s_j^2)} \quad j = 1,2$$

(21)

where $\phi(s_j)$ is the unknown function. Equation (18) can be replaced approximately by a series of algebraic equations based on Gauss–Chebyshev quadrature method. It can be written as

$$-\frac{\pi}{c}\sigma_{mn}^i(t_{iK}) = \sum_{j=1}^{5}\sum_{I=1}^{N}W_jR_j\left\{\phi_{x_j}(s_{jI})G_{x_jmn}^{ji}(s_{jI},t_{iK}) + \phi_{y_j}(s_{jI})G_{y_jmn}^{ji}(s_{jI},t_{iK})\right\}$$

$$mn = xy \, or \, yy$$

(22)

where

$$s_{1I} = s_{2I} = \cos[\pi I/(N+1)] \quad I = 1,2,\ldots,N$$
$$s_{3I} = s_{4I} = s_{5I} = \cos[\pi(2I-1)/2N] \quad I = 1,2,\ldots,N$$
$$t_{1K} = t_{2K} = \cos[\pi(2K-1)/(2N+2)] \quad K = 1,2,\ldots,N+1$$
$$t_{3K} = t_{4K} = t_{5K} = \cos[\pi K/N] \quad K = 1,2,\ldots,N-1$$
$$W_3 = W_4 = W_5 = 1/N; \quad W_1 = W_2 = (1-s_2^2)/(N+1)$$

(23)

The extra equations must be established to solve Eq. (22). Notice that there is no net dislocation on the macro-crack and the micro-cracks.

$$\sum_{I=1}^{N}\phi_{x_j}(s_{jI}) = \sum_{I=1}^{N}\phi_{y_j}(s_{jI}) = 0 \quad j = 3,4,5$$

(24)

So Eq. (22) can be solved. PZ size p_1 and p_2 can be obtained and $\phi(s_{jI})$ can be known. Further, the dislocation density functions $B(s)$ of PZ can be obtained by Eq. (21) where

$$\phi(s_j) = \frac{2}{N+1}\sum_{I=1}^{N}\left[\sum_{h=0}^{N-1}\sin\left[\frac{I\pi}{N+1}\right]\sin\left[\frac{I\pi}{N+1}(h+1)\right]\right.$$
$$\left.\frac{\sin[(h+1)\arccos(s)]}{\sin[\arccos(s)]}\right]\phi(s_{jI})$$

(25)

Results and discussion

In this section, PZ of the right macro-crack tip is only analyzed. The results of macroscopic analysis and microscopic analysis are shown as follows.

Macroscopic analysis of PZ

Comparison between theoretical and experimental results

In this section, the case is considered that an infinite plane contains only a center crack without micro-cracks under uniaxial tensile load. The comparison between theoretical and experimental results is shown in Fig. 3. The crack is located in $-1 \le x/a \le 1$. The parameter a is the half length of the crack. Due to the symmetry, only the upper half part of PZ is shown.
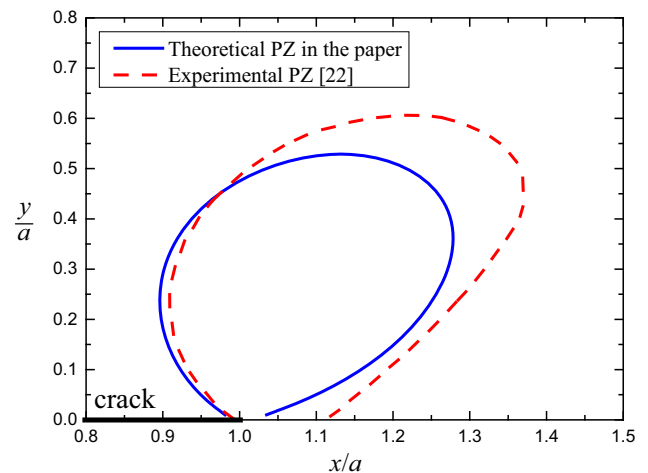
Figure 3 Comparison between theoretical PZ in this paper and experimental PZ.

Figure 4 Variation of PZ versus the location of the parallel micro-crack ($\alpha = 0°$).
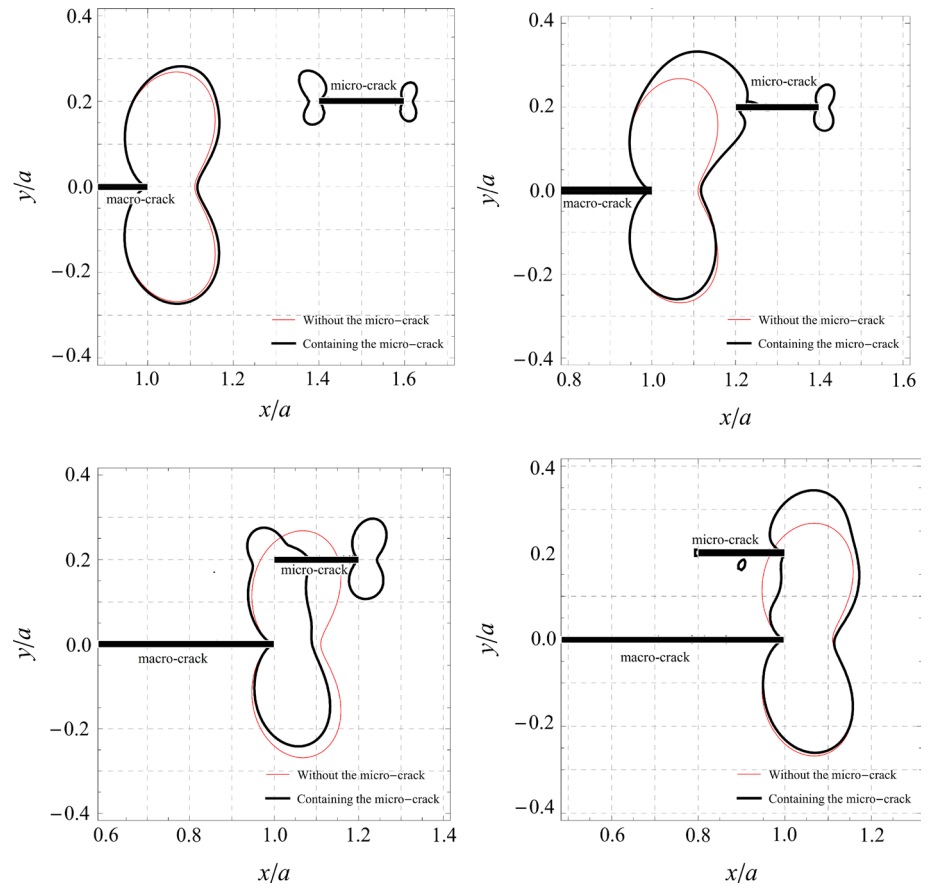
The experimental result was obtained under the conditions of 2024-T3 Alclad specimen of size ($420 \times 410 \times 1$ mm) containing a center crack subjected to uniaxial tensile load. The crack length to sheet width ratio is 0.25. The applied stress to the yield limit ratio is 0.6. The experimental result of PZ boundary was determined based on Tresca yield criterion. Compared with the experimental conditions, the theoretical result in Fig. 3 is obtained by Tresca yield criterion. And σ^∞ / σ_f is also taken as 0.6.

The results show that the shape of PZ in the paper is similar to the experimental result, and the size of PZ is slightly smaller than the experimental result. So the method in the paper can be applied to predict PZ.

The effect of the micro-crack on PZ

The stress field can be obtained by Eq. (13), and PZ is determined by von Mises yield criterion. σ^∞ / σ_f is taken as 0.5. a is half length of the macro-crack. Half length of the micro-crack is taken as $0.1a$.

The variation of PZ shape and size versus the location of the micro-crack is shown in Figs. 4 and 5. The red line denotes the boundary of PZ in the case that an infinite plane contains only the macro-crack without the micro-crack, and the thick black line denotes the boundary in the case that an infinite plane contains a micro-crack and a macro-crack.

In order to explain the results in Figs. 4 and 5 clearly, the case is considered that an infinite plane contains only a center crack. The contour representation of the normalized stress $\sigma_{yy}/\sigma^\infty$ is shown in Fig. 6. The white region denotes the stress shielding, and the gray region denotes the stress amplification.

The results in Figs. 4 and 5 show that the micro-crack has a little amplification effect on PZ of the macro-crack tip when it locates in front of PZ of the macro-crack tip. This is because the macro-crack locates in the stress amplification regions of the micro-crack. As the micro-crack is close to PZ of the macro-crack tip, PZ of the macro-crack tip and the

Figure 5 Variation of PZ versus the location of the inclined micro-crack ($\alpha = 30°$).

Contour representation of normalized stress figure:
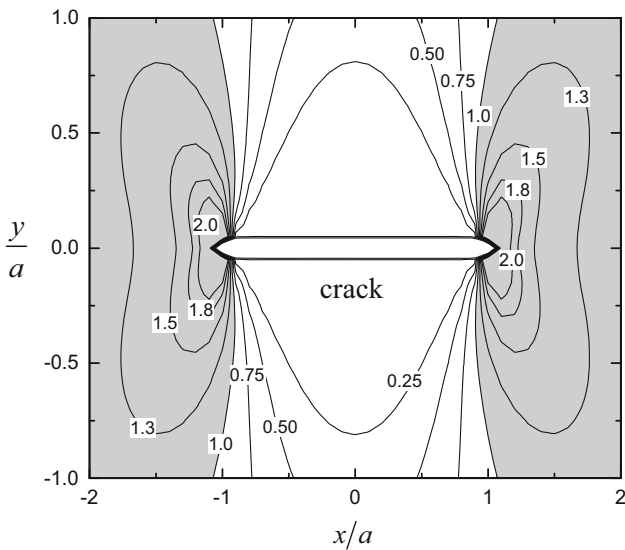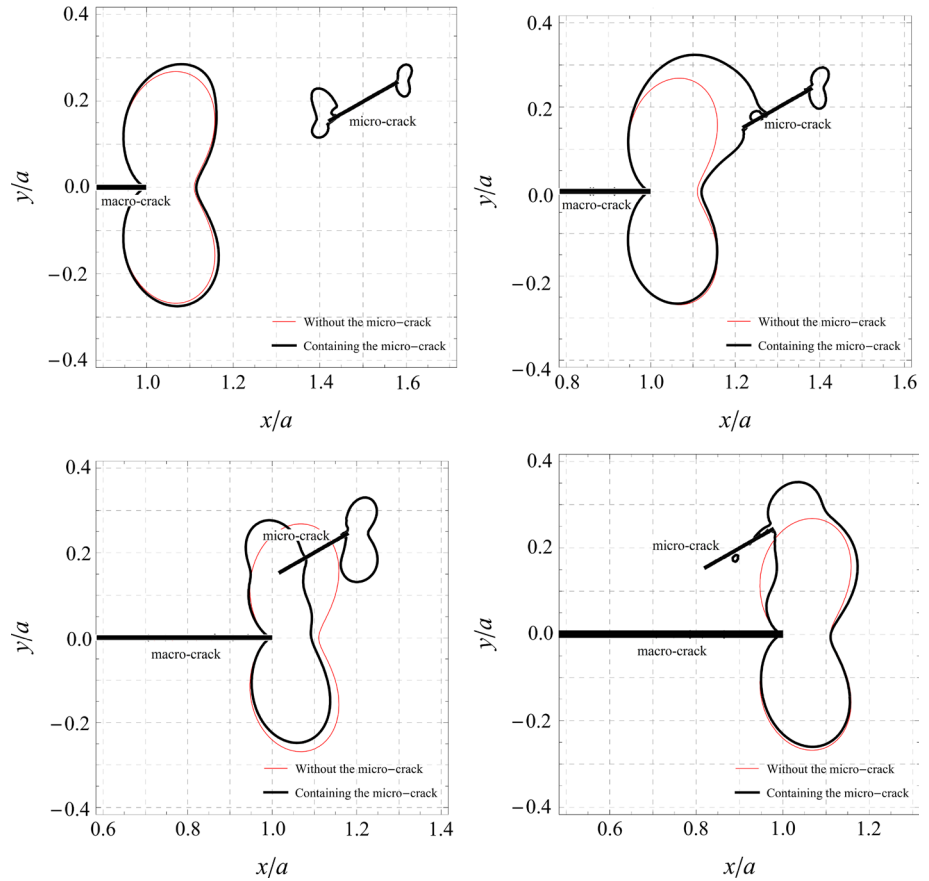
Figure 6 Contour representation of normalized stress $\sigma_{yy}/\sigma^{\infty}$ for a center crack in an infinite plane.

obvious shielding effect on the plasticity of the macro-crack tip. This is because the macro-crack tip locates in the stress shielding regions of the micro-crack. The stress field near the macro-crack tip is relaxed by the micro-crack. When the micro-crack is behind the macro-crack tip, it decreases the width of PZ but increases the height. On the whole, in the case, the micro-crack has a little effect on PZ size of the macro-crack tip. Comparing Figs. 4 and 5, it can be observed that the micro-crack angle has a little effect on PZ of the macro-crack tip.

For LEFM, the stress field near the crack tip is obtained based on Williams [49] expansion, and the first-order term of Williams expansion is considered only. But some recent works [50–53] shown that the high-order terms of Williams expansion had a significant effect on the stress field and the crack propagation. The stress field based on DDT is the complete stress field, so the results of PZ in the paper are more precise. However, the stresses will redistribute as the plasticity generates due to stress relaxation. So PZ in this paper by the yield criterion is an approximate value.

micro-crack tip will join together. PZ of the macro-crack tip increases drastically. When the micro-crack enters into PZ of the macro-crack tip, it has an

Microscopic analysis of PZ

Comparison and analysis about PZ size

Considering the case that an infinite plane contains a center crack under uniform tensile load, the results of PZ size are obtained by different methods, as shown in Fig. 7.
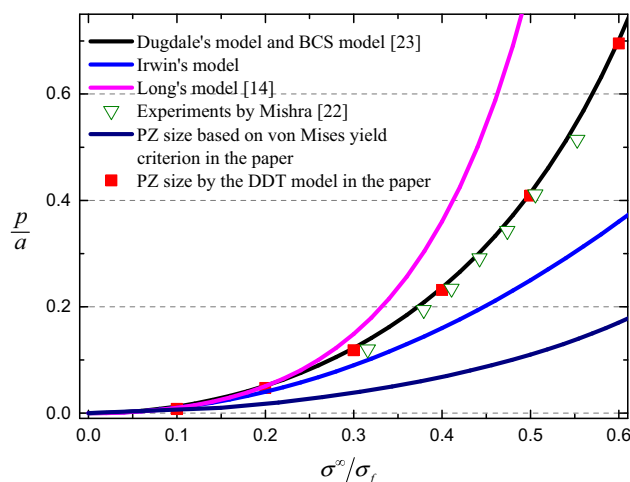
The variation of normalized PZ size p/a versus the applied stress level under remote uniform tensile load is depicted, and the comparison between the theoretical results and the experiment results is shown in Fig. 7. The results obtained by Dugdale model are same as BCS model, and the formula for calculating PZ size is given by

$$p = a\left[\sec\left(\frac{\pi\sigma^{\infty}}{2\sigma_f}\right) - 1\right] \quad (26)$$

The experimental results were obtained under the conditions of 2024-T3 Alclad specimen of size ($420 \times 410 \times 1$ mm) containing a center crack subjected to uniaxial tensile load. PZ size by experiments is the distance from the crack tip to the farthest point of PZ boundary.

The stresses are obtained by DDT, as shown in Fig. 6. PZ size along the crack line can be calculated based on von Mises yield criterion under plane stress condition. The results in this paper are obtained by von Mises yield criterion without considering stress relaxation, so it is smaller than other results.

The results in Fig. 7 show that the results are very close among Dugdale model, BCS model, the experiments and the DDT model. So it is reasonable that the DDT model is applied to calculate PZ size. The following results are obtained by the DDT model.

### Influence of micro-cracks on dislocation distribution at the macro-crack tip

In order to view clearly, the schematic diagram of the micro-cracks and the macro-crack is shown in Fig. 8.

As analyzed above, PZs are modeled as an array of continuously distributed edge dislocations. The dislocation density function can show the status of dislocation distribution in PZ, and it is plotted as follows.

The variation of normalized dislocation density versus the position x/a_1 under remote uniform tensile load for different applied stress level is depicted in Fig. 9. The other parameters are $d/a_1 = 3$, $a_2/a_1 = 0.3$, $\alpha = 0°$ and $\theta = 30°$. The results show that the dislocations are in the form of inverse pileup, which is consistent with previous observations by
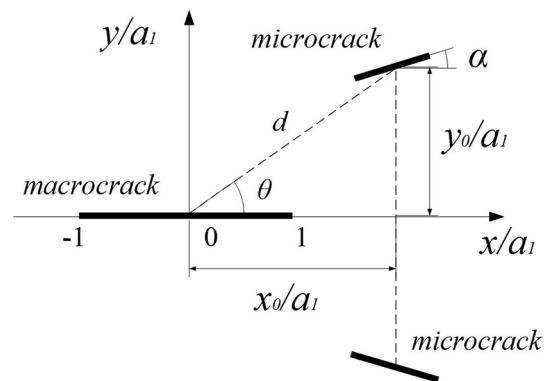
Figure 8 Schematic diagram of the micro-cracks parameters.

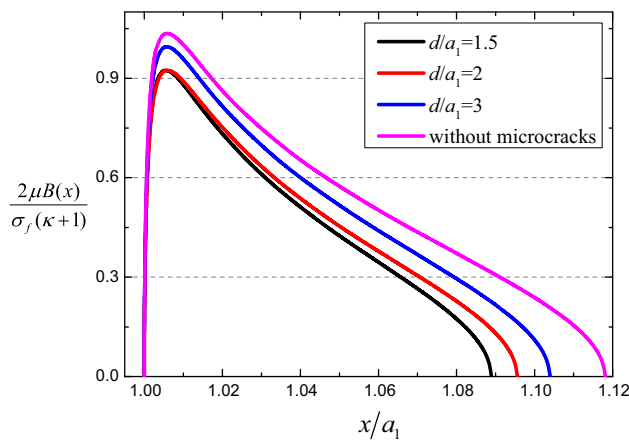Figure 7 Comparison about PZ size obtained by different methods.
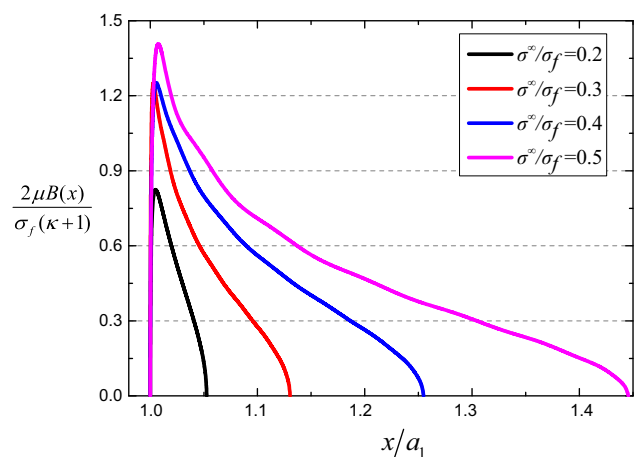
Figure 9 Normalized dislocation density function in PZ for different applied stress level.

experiments [18, 22]. The crack tip piles up a large amount of dislocations. As the applied stress increases, PZ size will increase dramatically, and the dislocations piled at the macro-crack tip will increase.

The variation of normalized dislocation density versus the location x/a_1 under remote uniform tensile load for different distance d/a_1 is depicted in Fig. 10. The other parameters are $\sigma^\infty/\sigma_f = 0.3$, $a_2/a_1 = 0.3$, $\alpha = 0°$ and $\theta = 60°$. The results show that the micro-cracks decrease PZ size. PZ size of the macro-crack tip decreases with the distance d/a_1 decreasing. In this case, the micro-cracks have a hindering effect on the dislocations omitted from the macro-crack tip.

The variation of normalized dislocation density versus the location x/a_1 under remote uniform tensile load for different micro-crack orientation θ is depicted in Fig. 11. The other parameters are $\sigma^\infty/\sigma_f = 0.4$, $a_2/a_1 = 0.3$, $\alpha = 0°$ and $d/a_1 = 3$. The results show that the micro-cracks have an amplification effect on PZ size at $\theta = 20°$, while they have a shielding effect at $\theta = 60°$ and $\theta = 80°$. The micro-crack orientation θ has a little effect on the dislocation pileup of the macro-crack tip.

The results in Figs. 9, 10 and 11 show that the dislocations are in the form of inverse pileup and the dislocation density at the both end of PZ are bounded, which is similar to dislocation distribution of the dislocation-free zone model. The dislocation density obtained by BCS model is infinite at the crack tip, which is not in conformity with the truth. So it is more proper that the DDT model is applied to analyze the dislocation distribution in PZ. However, for many materials, it is possible that several glide planes at the crack tip are activated simultaneously, and

then a broad PZ is formed. In this case, the dislocations are not distributed along the line of the macro-crack, and the DDT model cannot be applied to represent the shape of PZ, but it is still valid to calculate PZ size.

Influence of the micro-crack angle on PZ size

The variation of normalized PZ size versus the micro-crack angle under remote uniform tensile load for different micro-crack orientation is depicted in Fig. 12. The other parameters are $d/a_1 = 2$, $a_2/a_1 = 0.2$ and $\sigma^\infty/\sigma_f = 0.4$. p_0 is PZ size of the macro-crack tip without micro-cracks. The results show that the micro-cracks have a little effect on PZ size of the macro-crack tip at $60° < \alpha < 120°$. In this case, the inclination of the micro-cracks is relatively large, so
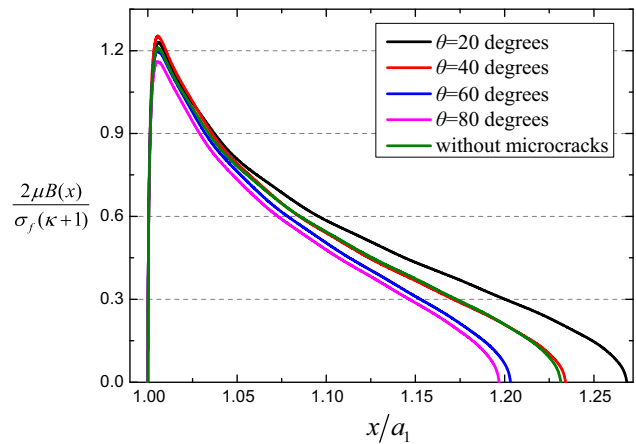
Figure 11 Normalized dislocation density function in PZ for different micro-crack orientation θ.

Figure 10 Normalized dislocation density function in PZ for different distance d/a_1.
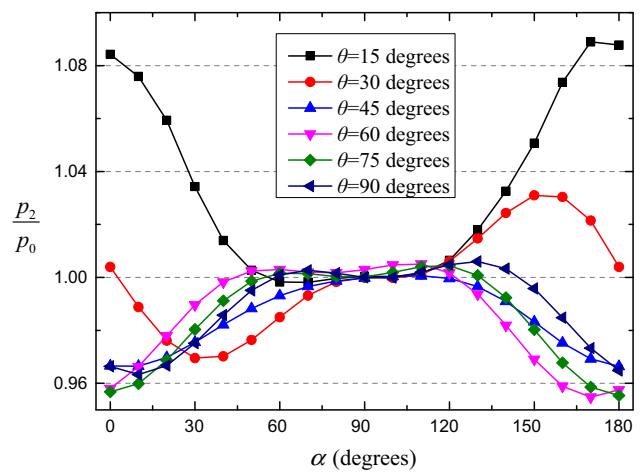
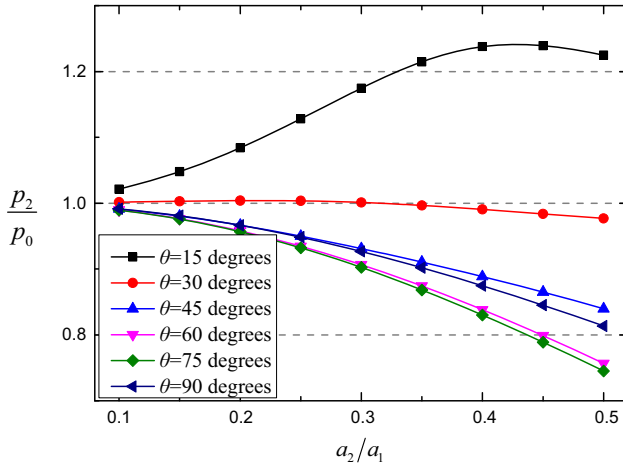**Figure 12** Normalized PZ size versus the micro-crack angle.

Figure 13 Normalized PZ size versus the micro-crack length.

the tractions on the micro-cracks face are relatively small. Hence, the micro-cracks have a little effect on the macro-crack. The effect of the micro-cracks on PZ size will get stronger as the inclination of the micro-cracks decreases at $0° < \alpha < 60°$ and $120° < \alpha < 180°$.

Influence of the micro-crack length on PZ size

The variation of normalized PZ size versus the micro-crack length under remote uniform tensile load for different micro-crack orientation is depicted in Fig. 13. The other parameters are $d/a_1 = 2$, $\alpha = 0°$ and $\sigma^\infty/\sigma_f = 0.4$. The results show that the effect of the micro-cracks on PZ size of the macro-crack tip will get stronger as the micro-cracks length increases.
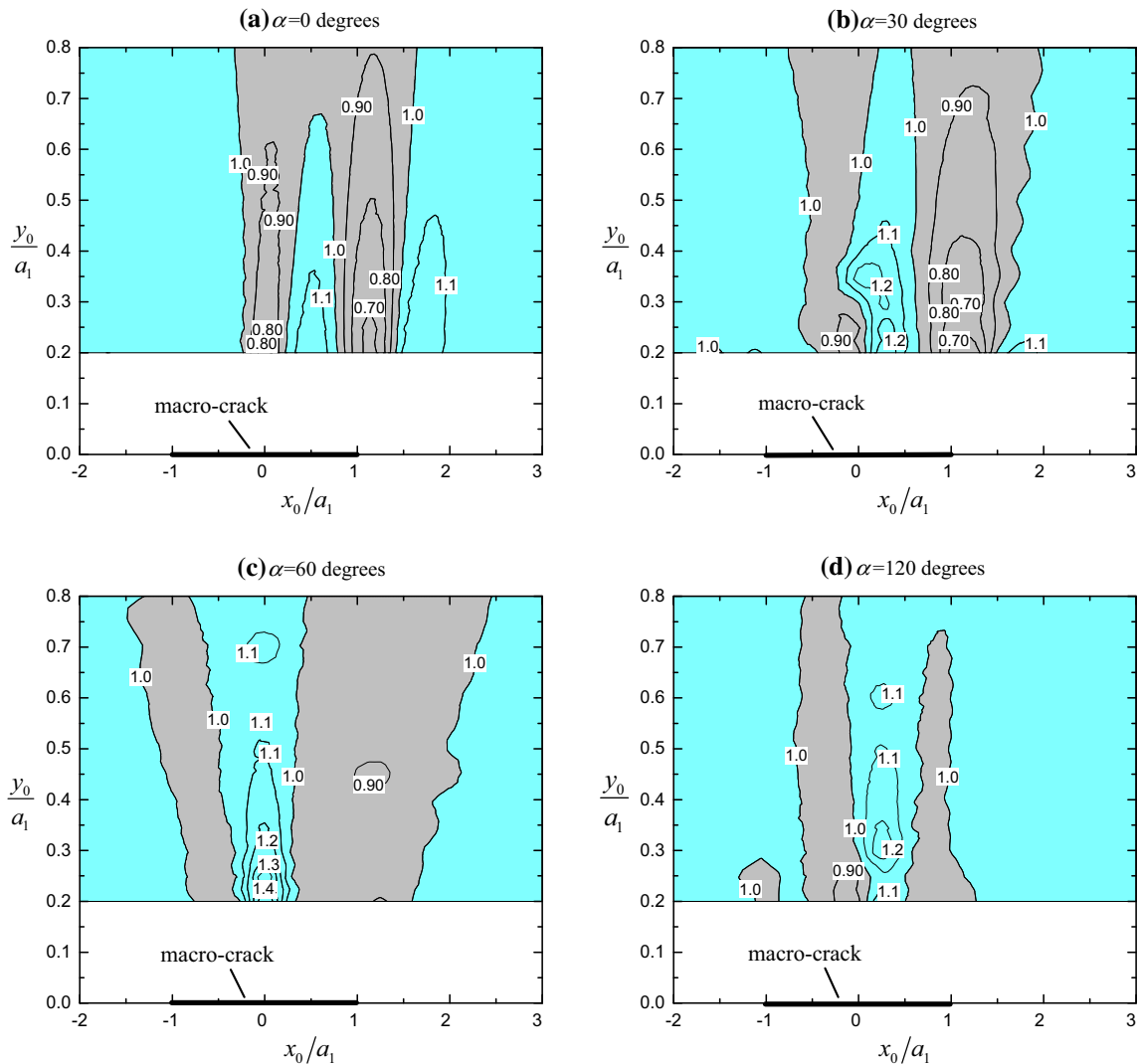

Figure 14 Contour chart of normalized PZ size p_2/p_0.

The micro-cracks increase PZ size at $\theta = 15°$, while they have a shielding effect on PZ size at $\theta > 30°$.

Next, the amplification and shielding effect of the micro-cracks on PZ size will be analyzed in detail.

Influence of the micro-crack location $(x_0/a_1, y_0/a_1)$ on PZ size

The variation of normalized PZ size p_2/p_0 versus the micro-crack location $(x_0/a_1, y_0/a_1)$ under remote uniform tensile load for different micro-crack angle is depicted in Fig. 14. The macro-crack is located in $-1 \leq x_0/a_1 \leq 1$. The other parameters are $a_2/a_1 = 0.2$ and $\sigma^\infty/\sigma_f = 0.4$. x_0/a_1 and y_0/a_1 are the horizontal distance and vertical distance between the macro-crack center and the micro-crack center, respectively, as shown in Fig. 8.

The micro-cracks have an amplification effect on PZ size in the cyan regions, and they have a shielding effect on PZ size in the gray regions. The results show that the amplification and shielding regions are divided into five strip-shaped regions, which are amplification, shielding, amplification, shielding and amplification region from left to right, respectively. The size and shape of shielding and amplification regions are different for the different micro-crack angle α. Considering the case of an infinite plane containing a center crack under uniaxial tension load, as shown in Fig. 6. Figure 6 shows that the stress concentration is produced near the crack tip and the stress shielding is produced in the bottom or top of the crack face, which is the reason that there are shielding regions when the micro-cracks are located in the bottom or top of the macro-crack. There are amplification regions when the micro-cracks are located in front of or behind the macro-crack. It can be observed that the micro-cracks have a little amplification effect on PZ size at about $x_0/a_1 < -1$ and $x_0/a_1 > 2$. This is because that the distance between the micro-cracks and the macro-crack is relatively large. At about $-1 < x_0/a_1 < 1$ and $0.2 < y_0/a_1 < 0.6$, the micro-cracks has a relatively large effect on PZ size.

Conclusion

In the paper, the problem of an infinite plane containing a macro-crack and micro-cracks is studied. PZ is determined based on macroscopic and microscopic methods. The dislocation density function in PZ is obtained. The effect of the micro-crack on PZ of the macro-crack tip is analyzed. Some conclusions can be summarized as follows.

1. When the micro-crack locates in front of PZ of the macro-crack tip, it has a little amplification effect on PZ of the macro-crack tip.
2. As the micro-crack is close to the macro-crack tip, PZ of the macro-crack tip and the micro-crack tip will join together.
3. When the micro-crack enters into PZ of the macro-crack tip, it has an obvious shielding effect on PZ of the macro-crack tip.
4. When the micro-crack is behind the macro-crack tip, it decreases the width of PZ but increases the height. On the whole, it has a little effect on PZ size.
5. The dislocation distribution in PZ is in the form of inverse pileup.
6. The effect of micro-cracks on PZ size will get stronger as the inclination of the micro-cracks decreases.
7. The effect of micro-cracks on PZ size will get stronger as the micro-cracks length increases.
8. The amplification and shielding regions are divided into five strip-shaped regions. And they appear alternately from left to right. The size and shape of the shielding and amplification regions are different for the different micro-crack angle.

The results in the paper can provide some useful information to predict the plastic behaviors in the macro-crack tip for the materials containing micro-cracks. What is more, the analysis of amplification and shielding regions is important to materials design.

References

[1] Rice JR, Rosengren GF (1968) Plane strain deformation near a crack tip in a power-law hardening material. J Mech Phys Solids 16(1):1–12

[2] Huang Y et al (2011) A new method of crack-tip opening displacement determined based on maximum crack opening displacement. Eng Fract Mech 78(7):1441–1451

[3] Codrington J, Kotousov A (2007) Application of the distributed dislocation technique for calculating cyclic crack tip plasticity effects. Fatigue Fract Eng Mater Struct 30(12):1182–1193

[4] Hom CL, Mcmeeking RM (1990) Large crack tip opening in thin elastic-plastic sheets. Int J Fract 45(2):103–122

[5] Sousa RA et al (2012) On improved crack tip plastic zone estimates based on T-stress and on complete stress fields. Fatigue Fract Eng Mater Struct 36(1):25–38

[6] Vasco-Olmo JM et al (2016) Assessment of crack tip plastic zone size and shape and its influence on crack tip shielding. Fatigue Fract Eng Mater Struct 39(8):969–981

[7] Xin G et al (2010) Analytic solutions to crack tip plastic zone under various loading conditions. Eur J Mech A Solids 29(4):738–745

[8] Nazarali Q, Wang X (2013) The effect of T-stress on crack-tip plastic zones under mixed-mode loading conditions. Fatigue Fract Eng Mater Struct 34(10):792–803

[9] Caputo F, Lamanna G, Soprano A (2013) On the evaluation of the plastic zone size at the crack tip. Eng Fract Mech 103(103):162–173

[10] Chen J et al (2014) A new method for cyclic crack-tip plastic zone size determination under cyclic tensile load. Eng Fract Mech 126:141–154

[11] Bouiadjra BB et al (2008) Analysis of the effect of micro-crack on the plastic strain ahead of main crack in aluminium alloy 2024 T3. Comput Mater Sci 42(1):100–106

[12] Bouiadjra BB et al (2009) Numerical estimation of the effects of microcavities on the plastic zone size ahead of the crack tip in aluminum alloy 2024 T3. Mater Des 30(3):752–757

[13] Paul SK (2016) Numerical models to determine the effect of soft and hard inclusions on different plastic zones of a fatigue crack in a C(T) specimen. Eng Fract Mech 159:90–97

[14] Korda AA, Miyashita Y, Mutoh Y (2015) The role of cyclic plastic zone size on fatigue crack growth behavior in high strength steels. In: International conference on mathematics and natural sciences

[15] Mishra SC, Parida BK (1985) Determination of the size of crack-tip plastic zone in a thin sheet under uniaxial loading. Eng Fract Mech 22(3):351–357

[16] Ding Y et al (2006) In situ TEM observation of microcrack nucleation and propagation in pure tin solder. Mater Sci Eng B 127(1):62–69

[17] Saka H, Agata Y (2003) Direct evidence for dislocation-free zone in Fe–5% Si fractured by Charpy impact test. Mater Sci Eng A 350(1):57–62

[18] Goswami R, Pande CS (2015) Investigations of crack-dislocation interactions ahead of mode-III crack. Mater Sci Eng A 627:217–222

[19] Ohr SM, Narayan J (1980) Electron microscope observation of shear cracks in stainless steel single crystals. Philos Mag A 41(1):81–89

[20] Horton JA, Ohr SM (1982) TEM observations of dislocation emission at crack tips in aluminium. J Mater Sci 17(11):3140–3148. doi:10.1007/BF01203476

[21] Kobayashi S, Ohr SM (1980) In situ fracture experiments in bcc metals. Philos Mag A 42(6):763–772

[22] Ohr SM (1985) An electron microscope study of crack tip deformation and its impact on the dislocation theory of fracture. Mater Sci Eng 72(1):1–35

[23] Bilby BA, Cottrell AH, Swinden KH (1963) The spread of plastic yield from a notch. Proc R Soc A 272(1350):304–314

[24] Chang SJ, Ohr SM (1981) Dislocation-free zone model of fracture. J Appl Phys 52(12):7174–7181

[25] Lung CW, Xiong LY (1983) The dislocation distribution function in the plastic zone at a crack tip. Phys Status Solidi 77(1):81–86

[26] Atkinson C, Kanninen MF (1977) A simple representation of crack tip plasticity: the inclined strip yield superdislocation model. Int J Fract 13(2):151–163

[27] Kanninen MF, Atkinson C (1980) Application of an inclined-strip-yield crack tip plasticity model to predict constant amplitude fatigue crack growth. Int J Fract 16(1):53–69

[28] Chen J, Takezono S (1995) The dislocation-free zone at a mode I crack tip. Eng Fract Mech 50(2):165–173

[29] Lee BH, Chung SK (1982) Semibrittle fracture instability in the inclined strip yield, continuum dislocation model. Mater Sci Eng 53(2):209–221

[30] Kachanov M (1985) A simple technique of stress analysis in elastic solids with many cracks. Int J Fract 28(1):R11–R19

[31] Kachanov M (1987) Elastic solids with many cracks: a simple method of analysis. Int J Solids Struct 23(1):23–43

[32] Chudnovsky A, Dolgopolsky A, Kachanov M (1987) Elastic interaction of a crack with a microcrack array—II. Elastic solution for two crack configurations (piecewise constant and linear approximations). Int J Solids Struct 23(1):11–21

[33] Gong SX, Horii H (1989) General solution to the problem of microcracks near the tip of a main crack. J Mech Phys Solids 37(1):27–46

[34] Gong SX, Meguid SA (1992) Microdefect interacting with a main crack: a general treatment. Int J Mech Sci 34(12):933–945

[35] Gong SX (1995) On the main crack-microcrack interaction under mode III loading. Eng Fract Mech 51(5):753–762

[36] Hori M, Nemat-Nasser S (1987) Interacting micro-cracks near the tip in the process zone of a macro-crack. J Mech Phys Solids 35(5):601–629

[37] Meguid SA, Gaultier PE, Gong SX (1991) A comparison between analytical and finite element analysis of main crack-microcrack interaction. Eng Fract Mech 38(6):451–465

[38] Ibbett J et al (2015) What triggers a microcrack in printed engineering parts produced by selective laser sintering on the first place? Mater Des 88:588–597

[39] Hills D et al (1996) Solution of crack problems: The distributed dislocation technique, 1996. Kluwer Academic Publishers, Dordrecht, pp 1–297

[40] Han J-J, Dhanasekar M (2004) Modelling cracks in arbitrarily shaped finite bodies by distribution of dislocation. Int J Solids Struct 41(2):399–411

[41] Zhang J et al (2014) Solution of multiple cracks in a finite plate of an elastic isotropic material with the distributed dislocation method. Acta Mech Solida Sin 27(3):276–283

[42] Li X et al (2016) Solution of an inclined crack in a finite plane and a new criterion to predict fatigue crack propagation. Int J Mech Sci 119:217–223

[43] Jin X, Keer LM (2006) Solution of multiple edge cracks in an elastic half plane. Int J Fract 137(1–4):121–137

[44] Li X, Li X, Jiang X (2017) Influence of a micro-crack on the finite macro-crack. Eng Fract Mech 177:95–103

[45] Chang D, Kotousov A (2012) A strip yield model for two collinear cracks. Eng Fract Mech 90:121–128

[46] Hoh HJ, Xiao ZM, Luo J (2010) Plastic zone size and crack tip opening displacement of a Dugdale crack interacting with a coated circular inclusion. Phil Mag 210(26):3511–3530

[47] Erdogan F et al (1973) Numerical solution of singular integral equations. In: Sih GC (ed) Methods of analysis and solutions of crack problems, Springer, pp 368–425

[48] Kaya AC, Erdogan F (1987) On the solution of integral equations with strongly singular kernels. Q Appl Math 45(1):105–122

[49] Williams M (1957) On the stress distribution at the base of a stationary crack. J Appl Mech ASME 24:109–114

[50] Roux-Langlois C et al (2015) DIC identification and X-FEM simulation of fatigue crack growth based on the Williams' series. Int J Solids Struct 53:38–47

[51] Mróz KP, Mróz Z (2010) On crack path evolution rules. Eng Fract Mech 77(11):1781–1807

[52] Larisa S, Pavel R, Pavel L (2016) A photoelastic study for multiparametric analysis of the near crack tip stress field under mixed mode loading. Procedia Struct Integr 2:1797–1804

[53] Malíková L, Veselý V, Seitl S (2016) Crack propagation direction in a mixed mode geometry estimated via multi-parameter fracture criteria. Int J Fatigue 89:99–107